Computational fluid dynamics for ameliorating oil recovery using silicon-based nanofluids and ethanol in oil-wet reservoirs

DOI:
10.1016/j.egyr.2020.10.028

Document Version
Final published version

Energy Reports 6 (2020) 3023–3035

Contents lists available at ScienceDirect

Energy Reports

journal homepage: www.elsevier.com/locate/egyr

Computational fluid dynamics for ameliorating oil recovery using silicon-based nanofluids and ethanol in oil-wet reservoirs

Chukwugozie Ejeh [a,b,*], Imran Afgan [a,c], Hamzah AlMansob [a], Eric Brantson [d], Joseph Fekala [b], Micah Odiator [b], Promise Stanley [b], Prosper Anumah [e], Chigozirim Onyekperem [f], Evans Boah [b]

[a] Department of Mechanical Engineering, School of Engineering, Khalifa University of Science and Technology, Abu Dhabi, P.O Box 127788, United Arab Emirates
[b] Department of Oil and Gas Engineering, School of Engineering, All Nations University, Koforidua, Eastern Region, P.O Box kf 1908, Ghana
[c] Department of MACE, School of Engineering, University of Manchester, Manchester, M13 9PL, United Kingdom
[d] Department of Petroleum Engineering, University of Mines and Technology, Tarkwa, P.O. Box 237, Ghana
[e] Department of Energy and Petroleum Engineering, University of Energy and Natural Resources, Sunyani, Brong Ahafo Region, P.O Box 214, Ghana
[f] Center of Excellence in Marine Engineering and Offshore Technology, Rivers State University, River State, Nkpolu - Oroworukwo P.M.B. 5080. Port Harcourt, Nigeria

ARTICLE INFO

Article history:
Received 3 June 2020
Received in revised form 27 September 2020
Accepted 20 October 2020
Available online xxxx

Keywords:
Computational fluids dynamics
Interfacial tension
Nanofluid
Enhanced oil recovery
Wettability alteration

ABSTRACT

Impulsive emulsion formation, porous media wettability alteration, and interfacial tension (IFT) reduction are a list of advantages gained from the application of nanoparticles for enhanced oil recovery (EOR). However, low displacement efficiency (DE) coupled with in-effective mixing of the injected nanofluid to redeem the immobile volume of crude oil subsurface present a major challenge to the petroleum industry. The molecular chemistry of ethyl alcohol (ethanol) solvent enables the genesis of strong covalent bonds/mixing with the dense oil. As a result, the fastening converts the aromatic state of the crude oil to a lighter component to ease the flow. In this paper, we numerically investigated the potential for improving dead oil recovery in a heterogeneous rock setting using a blend of ethanol and silicon-based nanofluids to describe the EOR fluid. Herein, silica, silane and silicon carbide nanofluids were studied for their DE with ethanol as the co-solvent. A 2D heterogeneous pore-model was created and discretized to define the computational domain. Computational fluid dynamics code (ANSYS Fluent) facilitated the induction and analysis of interfacial property dynamics within the modelling space. The simulation was performed using the improved delayed detached-eddy simulation method, whereas the continuum surface-force equation with the Euler–Euler mixture multiphase method was used to model the fluid–wall and fluid–fluid adhesions at interfaces. Findings revealed that, silica nanofluid performed optimally compared to its counterpart. Furthermore, approximately 55.34% of the immobile oil was recovered using the optimal blend formulation comprising of equal proportion of silica nanofluid and ethanol. The increase in disjoining pressure and water molecules concentration at the fluid–wall contact, and the reduction in interfacial tension due to the evolution of in-situ surface acting agents (surfactants) from the chemical reaction kenetics accounts for this increase. In addition, the blend demonstrated good thermal stability for typical reservoir temperatures of around 400 K due to high intrinsic thermal resilence of silica nanoparticles present in the mixture.

1. Introduction

The need for energy from fossil fuels to heat homes, electricity generation, power automotive engines among others have contributed to the growing search for methods to improve crude oil production in an economic, safe and environmentally friendly manner. Studies by Boah et al. (2019) communicate that, drilling infill wells at target locations to recover the trapped volumes of crude oil is cost implicating with only a little fraction being produced. Furthermore, low pressurization, loss of solution gas and the growing affinity for the formation rock surfaces to preferentially adhere to the non-wetting phase is a plausible cause for the decrease in petroleum reservoir's oil production history (Shedid, 2015; Fard et al., 2016; Youssif et al., 2018; Pal et al., 2018; Phukan et al., 2019; Al-Murayri et al., 2019; Boah et al.,

* Corresponding author at: Department of Mechanical Engineering, School of Engineering, Khalifa University of Science and Technology, Abu Dhabi, P.O Box 127788, United Arab Emirates.
E-mail address: echukwugozie@gmail.com (C. Ejeh).

https://doi.org/10.1016/j.egyr.2020.10.028

2019). Depending up on the areal extent and volumetric capacity of the reservoir, the volume ratio of the residual oil could range between 10%–30% (Phukan et al., 2019; Al-Murayri et al., 2019).

Chemical enhance oil recovery (EOR) with alkaline–surfactant–polymer injection, being one of the most used EOR technique, was estimated to recover about 70% of the original oil in place (OOIP) (Sheng, 2010, 2013; Sun et al., 2020; Rezaei et al., 2020). However, the loss in polymer viscoelastic property in high temperature and saline reservoir environment resulted to the reduced operational performance of the chemical (Jekwu, 2018; Huang et al., 2020). In addition to the above, polymer elongation coupled with the decline in interfacial connection coerced by alkaline/surfactant additives with the rock surface accounted for the remaining 30% OOIP (Li et al., 2019; Yang et al., 2019). Nanoparticles, are now extensively used for various engineering applications in recent years. For example, a wide variety of silica nanoparticle is adopted to amiliorate the thermal stability of base working fluids for solar thermal application (Abed and Afgan, 2019, 2020; Abed et al., 2020). Similarly, nanoparticles have been proven to achieve excellent chemical destabilization of oil–water emulsion, polymer thermal stability enhancement, and an improvement in EOR fluid contact efficiency to considerably reduce the occurrence of selective channelling of the injected substance. To begin with, Onyekonwu and Ogolo (2010) used poly-silicone nanoparticles, a type of hydrophilic nanoparticles, to revamp the displacement efficiency of chemical oil recovery fluids through sandstone porous channels. The nanofluid prepared from a proportional mixture of water, ethanol and silica nanoparticles depleted additional volumes of the trapped oil (Rezaei et al., 2020). Transmission electron microscope images confirmed the surface wetness modification and adsorption of nanoparticles on the rock surfaces (Ju and Fan, 2009; Zhang et al., 2011). Fereidooni Moghadam and Azizian (2014) used Zinc oxide (ZnO) nanofluid to augment the interfacial properties of anionic surfactants through repeated experiments. Research work by Suleimanov et al. (2011) informed that iron nanoparticles combined with surfactants could yield up to 35% of the left-behind OIP while Giraldo et al. (2013) prepared nanofluids from mixing aluminium oxide (Al_20_3) nanoparticles and surfactants to alter the oil-wetting tendency of the sandstone core samples for improved oil recovery. Furthermore, Roustaei et al. (2012) outlined that a measurable reduction in surface tension (26 to 2 dynes/m) could be arrived at when administering silicon-based nanofluids downhole into the oil-rich zone. The performance of the novel mixture was highly esteemed at the end of their investigation to be better than other types of metal oxide nanoparticles. Recently, Kim et al. (2019) experimentally characterized the effect of nano-acid fluids to oil recovery amelioration in tight carbonates reservoirs. Three nano-acid chemicals composed of using $Si0_2$-acid, Al_20_3-acid, and ZnO-acid were considered. Results from their analysis depicts that $Si0_2$-acid achieved a greater success in dealing with high IFT issues, and it displaced a substaintial amount of the residual oil (Kim et al., 2019). Findings confirm that, nanoparticles have the potential for optimizing the functionality of fluids in this perspective, and in other engineering applications. The increase in disjoining pressure at the fluid-solid contacts, given rise to by the presence of nanoparticles in the injected chemical solution. As a consequence, it considerably overcame the adhesive forces that originally held the crude oil bound to the surface of the rock. Furthermore, the invaded nanoparticles forms a wedge-like structure at the solid interfaces due to prevailing molecular randomization and electrostatic repulsion (El-Diasty and Aly, 2015; Al-Anssari et al., 2016; Youssif et al., 2018). Hence, the chemistry of the rock surface becomes polarized and attracts negatively charged compounds such as the hydroxide ion group commonly found in ionized water (Kazemzadeh et al., 2019). However, the viscosity of the dead oil remains unchanged. The effectiveness of conventional EOR methods are limited thereby requiring additives to reduce the oil's density through effective mixing and at the same time, curbs the oil-wetting proneness of the reservoir rocks. The injection of supercritical fluids such as Carbondioxide (CO_2), methane (CH_4) and the likes were proposed in literature to reduce the aromatic state of the residual oil to ease the flow. However, they are relatively costly and operationally unstable compared to ethanol (C_2H_60), a type of biofuel. Ethanol has shown to be the choice of additive over supercritical fluids to solve the problem. The excellent oil cleaning properties of ethanol gives it the advantage to be commercially adopted as the key reagent for soap making. Adding to this, ethanol has the propensity to initiate a stable and strong single covalent bonding with hydrocarbons irrespective of their classification. The fusion shrinks the densisy and viscosity of the heavy oil. A hydrogen bond from the double bonds holding the complex hydrocarbon molecules together breaks away and connects with a carbon atom in ethanol. The process continues with time with increasing ethanol concentration. It should be noted that, water molecules are fashioned as a bi-product from the chemical interaction. Ethanol has also gained great success in oil-spill cleaning at the river banks or sea shores. However, their volatility in high temperature envirmonment similar to those experienced in petroleum reservoirs is of great concern. Blending ethanol witha thermally stable substance or additive could help solve the problem (Abed and Afgan, 2020).

Ferreira et al. (2020) disclosed in their work that, ethanol (biofuel) is an excellent emulsion destabilizer, and Safaei et al. (2020) showed through experiments that nanofluids prepared from ethanol and nanoparticles heighten non-associated gas production in gas-condensate reservoirs by flushing-out endcaped gas molecules within the pore spaces. In addition, Al-Maskari et al. (2019) studied the effectiveness of ethanol in altering the oil-wetting harmony of carbonates formations. The experimental setups were created to study the problem using alcohol-assisted water flooding approach. Experimental methods, which are very cost-intensive, time consuming and permits very limited room for repeated trails, have been employed so far to study this problem. Numerical methods such as computational fluid dynamics (CFD) codes is well known to bestow a more cost-effective to investigate EOR issues and other applications with a great deal of accuracy (Van Hooff et al., 2017). Furthermore, CFD technique warrant its users critical insights on the prevailing multiscale fluid dynamic processes taking place between the interacting phases, leading to the improvement in oil recovery. One major setback with the use of advanced CFD codes to solve the continuity and momentum equation and energy balance equation is the need for high computing power and space. The computational requirement increases with the complexity of the problem (Norton and Sun, 2006; Benhamadouche et al., 2019; Alam et al., 2017; Rezaeiha et al., 2019). A typical example is the direct numerical simulation approach (Wu et al., 2017a,b, 2019) judged to have great success in accurately predicting flow variables compared to large eddy simulation method (LES), hybrid Reynolds-averaged Navier Stokes (RANS)–LES model, and the RANS approach in that order. Nguyen et al. (2019), Revell et al. (2020) and Ejeh et al. (2020a) reported that, hybrid RANS–LES turbulence modelling method is relatively less costly in terms of computational requirements, and yields accurate numerical solutions, making it suitable especially for problems involving separated shear layers due to adverse pressure gradients and large-scale fluctuations, and high Reynolds (Re) number attached boundary layer flows (Delafin et al., 2017; Xu et al., 2018; Filippone and Afgan, 2008; Paterson and Peltier, 2005).

CFD codes have been used recentlly to study EOR related issues. Rostami et al. (2019) and Jafari et al. (2019) studied the

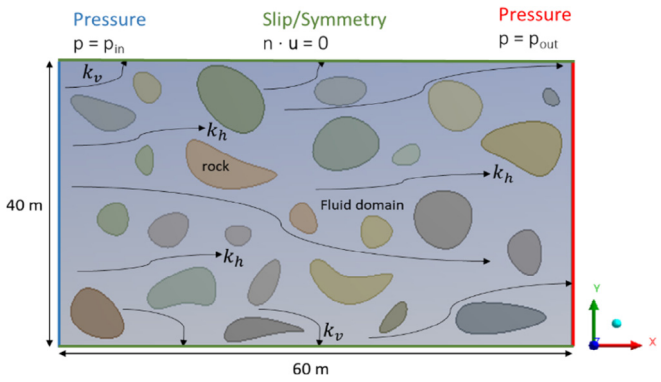

Fig. 1. Infinite model geometry showing flow and no-flow regions.

effect of nanoparticles on wettability alteration through the reduction of IFT for EOR in oil-wet reservoirs through CFD analysis. Druetta (2019) numerically improved the performance of chemical EOR method (Polymer flooding) using SiO_2 nanoparticles. Furthermore, CFD was employed by Gharibshahi et al. (2019) to decrease the viscosity of heavy oil from 35 Pa s to 25 Pa s using different nanofluids.

In this paper, CFD code in the commercial software ANSYS is used to evaluate the potential of ethanol to enhance EOR fluids performances. Here, different mixtures made of silane, silica and silicon carbide nanoparticles with ethanol solvent are compared. The effect of concentration and temperature are considered in the numerical investigation. Turbulence is modelled using the non-zonal HRL (IDDES) method, and the mixture model is activated to resolve the volume fraction equations for each transported phases, while the continuum surface-force equation takes care of interfacial interactions during the time dependen flow resolution.

2. Method and materials

2.1. Model creation

A two dimension (2D) rectangular geometry which represent the part to be discretized is created using ANSYS Geomodeler tools. The areal extent of the model is 40×60 m. The geometry highlights a tiny portion of a typical petroleum reservoir. The irregularly-shaped patches seen in Fig. 1 is distributed randomly and subtracted from the rectangular sketch using the Boolean function. This is aimed at creating no-flow or solid boundaries to include gross heterogeneities within the finite element model. As a consequence, the flow path of the transmitted fluid becomes non-linear rather than linear. This way, we made an attampt to mimic typical reservoir formation charateristics with respect to porosity and permeability. A sketch of the ideal flow trajectories: vertical permeability k_v and horizontal permeability k_h are conveyed in Fig. 1. It is a rough description of the fluid's track. However, in the finite element model, the fluid pathline and turbulent movement of the interpenetrating phases are entirely governed by the implemented numerical models. Moreover, the geomtry shows assigned boundaries, and modeling conditions at bounded regions. Once the part has been created, the next step is to create the modeling space. This is done by discretizing the infinitely large part into small finite elements.

2.2. Discretization Process

Meshing is essential in any CFD investigation to reduce the degrees of freedom from infinite to a finite number to allow the solvers to make calculations/predictions at each node and cell face of the finite element. In general, the choice of meshing strategy do have an impact on the computational process, solution accuracy, and convergence rate. In light of this, a fine and structured mesh is distributed throughout the infinite model while using CFD as the physics preference. Furthermore, a triangular-free face mesh was created using the quadrilateral-dominant method with disfeaturing size, curvature angle and a body size of 0.00146 mm, 2° and 0.3 mm, respectively. Ten (10) boundary layers with first-layer thickness of 0.4 mm is constructed by a growth rate of 1.2 near the boundaries encompassing the irregular patch body which describes the porous media matrix as displayed in Fig. 2. Furthermore, a grid independent study is carried-out to ensure that the adopted discretization process is valid for the problem as informed by Ejeh et al. (2019, 2020a,b,c), where critical insights on the impact of meshing parameters was exposed. In the mesh sensitivity process, the predicted velocity magnitude is recorded for every increment in the number of elements. The outcomes are plotted as exhibited in Fig. 3. It can be observed that the solutions tend to converged for higher number of elements. In total, 83,479 elements were generated at the end of the process, and this number lied within the convergence region.

2.3. Materials and boundary conditions

Crude oil with API gravity of 35° (Ejeh et al., 2020d), ethanol and nanoparticles (in solution state) or nanofluids are used for the investigation. The mixture of the last two substances is given the name E-N. Details of the individual fluid properties obtained from ANSYS material database are listed in Tables 1 and 2. Here, silane, silica and silicon carbide materials in the liquid state are used to represent the nanofluid to be blended with ethanol. The reason behind their selection is due to the imcreasing application of silicon-based nanofluids to boost the performances of engineered

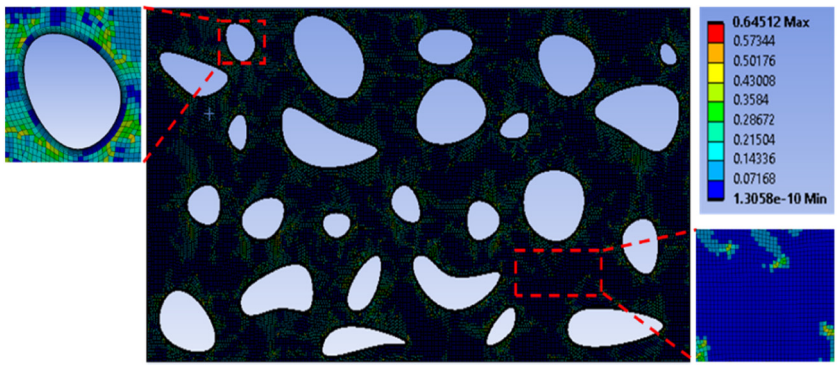

Fig. 2. Geometry discretization detailing the treatment of boundary layers and flow media.

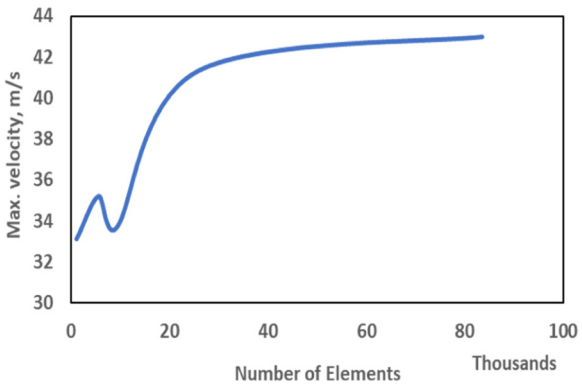

Fig. 3. Grid independence plot.

Table 1
Crude oil and ethanol properties (ANSYS Fluid database, 2019).

Properties	Crude oil (n-octane)	Ethanol ($\mathbf{C_2H_5OH}$)
Density	850 Kg/m^3	790 Kg/m^3
Specific heat	2,420 J/kg-k	2,470 J/kg-k
Thermal conductivity	0.147 W/m-k	0.182 W/m-k
Viscosity	0.00054 Kg/m-s	0.0012 Kg/m-s
Molecular weight	114.1502 Kg/k-mol	46.07 Kg/kmol
Latent heat	306,446 J/kg	855,237 J/kg
Vaporization temperature	292 K	271 K
Boiling point	399 K	351 K
Binary diffusivity	5.0510^{-06} m^2/s	1.3710^{-05} m^2/s
Saturation vapour pressure	1,329 Pa	7,974 Pa
Droplet surface tension	0.021213 dynes/m	0.022348 dynes/m

fluids. The materials properties are assigned to the model prior to setting-up the boundary informations.

To model surface behaviour of the fluids within the computational space, the continuum surface-force equation with wall adhesion option is selected in the process of setting up the multiphase flow model. Furthermore, the continuum surface-force model engages a systematic interpretation of the changing surface tension during the time-dependent simulation run rather than using a single boundary value throughout the run. The initial surface tension coefficient acting at nanofluid–crude oil, ethanol–crude oil, and ethanol–nanofluid interface are 0.016, 0.038, and 0.0013, respectively. Moreover, the surface tension coefficient between the nanofluid and ethanol is made very small to allow effective mixing. In addition, the wall adhesion option is selected to cause the crude oil to make adequate contact with the wall surfaces. Note that, the nanofluid and ethanol are introduced from the inlet with common a velocity of 1 m/s, while the crude oil material properties is assigned to the flow domain with an ignition velocity as low as $\times 10^{-5}$ m/s. In addition, the outlet pressure P_{out} is set to zero to achieve maximum pressure gradient around that section.

The pressure-Implicit with Splitting of Operators (PISO) pressure–velocity coupling scheme is implemented for higher degree corrections of pressure and velocity predictions. In contrast to the SIMPLE and SIMPLEC approach, the PISO algorithm satisfies the conservation of momentum after solving the pressure corrections. Furthermore, the PISO method performs two more corrections: that is, the skewness corrections and neighbourhood corrections. The PISO algorithm assume these processes to improve the pressure and velocity corrections calculations. We reduced the convergence criterion to nine (9) decimal places to allow the solution to converge with the second-order discretization schemes formulation. The calculation is set to run for two hundred (200) time steps with ten (10) iterations for every step size of 0.01s. A small step size is essential to have a detailed visual of the flow transition, and to avoid floating points report due to solution divergence.

2.4. Turbulence modelling

Turbulence model is crucial for every CFD analysis to treat flow of each transported phases. Here, we made use of the improved delayed detached eddy simulation (IDDES) method to accurately predict the mean skin friction for wall-bounded subsonic flow with relatively less computational efforts. IDDES is a hybrid of the RANS method and the LES approach (Jamal et al., 2018). It is solely time-dependent procedure solves the conservation equation for each phase independently. The momentum equation is shown in Eq. (1) where u_i and $\hat{u}_i\hat{u}_j$ describes the instantaneous velocity and filtered velocity, respectively, and $\frac{\partial}{\partial x_j}(\tau_{ij})$ is the turbulent stress component which can be resolved using Eq. (2) (Alam et al., 2017). It relates the total residual stress tensor derived through filtration of the momentum equation or Reynolds averaging.

$$\frac{\partial \hat{u}_i}{\partial t} + \hat{u}_j \frac{\partial \hat{u}_i}{\partial x_j} = -\frac{1}{\rho}\frac{\partial \hat{p}_i}{\partial x_i} + \frac{\partial}{\partial x_j}\left(2\upsilon \hat{s}_{ij}\right) - \frac{\partial}{\partial x_j}\left(\tau_{ij}\right) \quad (1)$$

$$\tau_{ij} = \widehat{u_i u_j} - \hat{u}_i\hat{u}_j \quad (2)$$

In addition to the previous discussion, a scalar variable is used in the filtered momentum equation for the sole purpose of modelling turbulent stress based on the Boussinesq hypothesis. This term is given the name eddy viscosity. Theoretically, this term assumes a numerical value appropriate for a modelled Reynolds stress at the RANS near the wall and does the same for a modelled sub grid stress far from the wall (Jamal et al., 2018; Ahmed et al., 2020). Moreover, studies have proven that combining the effect of spatial filtered, and ensemble average velocity fields with the aid of a single scalar variable introduce discrepancy or inaccuracy into the modelling process. Based on this, the DHRL modelling approach makes the attempt to address this issue (Shobayo and Walters, 2018). The process begins with the decomposition of the velocity field. When this happens, the spatially filtered and ensemble averaged velocity fields obtain different values in the transition region. The first stage is to introduce the decomposition

Table 2
Nanoparticles types and modeling parameters (ANSYS Fluid database, 2019).

Properties	Silane ($\mathbf{SiH_4}$)-powder	Silica ($\mathbf{SiO_2}$)-powder	Silicon carbide (**SiC**)-powder
Density (powder)	3.185 Kg/m^3	2.650 Kg/m^3	3.210 Kg/m^3
Specific heat	Piecewise-polynomial	Piecewise-polynomial	Piecewise-polynomial
Drag law	Spherical	Spherical	Spherical
Molecular weight	32.118 Kg/k-mol	28.086 Kg/k-mol	40.097 Kg/k-mol
Standard state enthalpy	3.389×10^{07}J/kg-mol	4.5063×10^{08} J/kg-mol	7.1971×10^{08} J/kg-mol
Standard state entropy	204,594.7 J/kg-mol-k	167,863.6 J/kg-mol-k	213,110.8 J/kg-mol-k
Reference temperature	298 K	298 K	298 K
Particle diameter	1×10^{-05} m	1×10^{-05} m	1×10^{-05} m
Radial distribution	Lun et al.	Lun et al.	Lun et al.
Injection rate	1 kg/s	1 Kg/s	1 Kg/s

for the instantaneous velocity u_i calculated from Eq. (3), where u_i'' is the i-component of the resolved fluctuating velocity, u_i' is the unresolved fluctuating velocity, $\widehat{u_i u_j}$ and $\overline{u_i}$ are the simulation resolved velocity, and Reynolds-averaged velocity, respectively (Alam et al., 2017).

$$u_i = \overline{u_i} + u_i'' + u_i' \text{ and } \hat{u}_i = \overline{u_i} + u_i'' \tag{3}$$

The turbulent stress term is used to define the modelled fluctuating velocity. By inserting the decomposed instantaneous velocity u_i into Eqs. (2) and (3), results in an expression for residual stress is provided below.

$$\tau_{ij} = (\widehat{\hat{u}_i \hat{u}_j} - \hat{u}_i \hat{u}_j) + \widehat{u_i' u_j'} \tag{4}$$

A subfilter is obtainable through the scale similarity concept for the modelling of both terms at the right-hand side of Eq. (3). The relationship of the subfilter is shown in Eq. (6).

$$\tau_{ij} = \alpha(\widehat{\hat{u}_i \hat{u}_j} - \hat{u}_i \hat{u}_j) + \beta \overline{u_i' u_j'} \tag{5}$$

With regards to Eq. (5), both the first and second term at the right can be linearized as functions of the subgrid stress (SGS) and ensemble-averaged in that order. These stress terms are derivable from SGS and RANS models, respectively (Jamal et al., 2018). The terms α and β represent proportionality constant, which may be constant or vary. However, they are most times considered complementary with the notion that the residual stress term is defined as a weighted average of the SGS and RANS stress as provided below (Alam et al., 2017).

$$\tau_{ij} = \alpha \tau_{ij}^{SGS} + (1-\alpha)\tau_{ij}^{RANS} \tag{6}$$

The blending coefficient can be determined from the relationship below, by applying a secondary filtering operation similar to Lilly (1992) for the evaluation of dynamic model coefficient for subgrid stress modelling.

$$\alpha = u_i'' u_j'' \overline{S_{ij}} / \tau_{ij}^{RANS} \overline{S_{ij}} - \tau_{ij}^{SGS} \overline{S_{ij}} \tag{7}$$

In practice, the value of the blending coefficient stability lies between 0 and 1. Regions with no resolved fluctuations have a value of 1, which is a steady-state condition. Here, pure RANS modelling is achieved (Jamal et al., 2018). However, areas at which the velocity fluctuations are resolved, α value is increased to 1 (Spalart et al., 2006; Shur et al., 2008). Hence, pure LES is attained. This dynamic value of α ensures that a smooth transition from RANS-to-LES is achieved during the simulation process (Shobayo and Walters, 2018).

2.5. Multiphase flow modelling

The mixture method is implemented for modelling mixture of multiple interacting fluids based on their volume fraction. In general, the mixture model makes use of a single-fluid approach, just like the volume of fluid (VOF) method (Mishra et al., 2019). However, the mixture method allows the phases to interpenetrate with each other, which is not the case with the VOF method. Secondly, the control volume fractions β_q and β_p could assume any value between 0 and 1 (Madhania et al., 2017). The parametric worth of β_q and β_p depends largely upon the space engulfed by the primary phase q (crude oil) and secondary phase p (injected fluid), respectively. Furthermore, each phase during the simulation run is permitted to propagate at different velocities when using the mixture model with appropriate boundary conditions at the no-flow zones; that is the slip boundary condition, making the flow process dynamic and comparable to real world scenarios (Madhania et al., 2017). In addition, the used multiphase flow method solves the momentum equation, continuity equation, and energy equation for the secondary phases (nanofluid and ethanol) whilst that of crude oil is treated by IDDES turbulence model. Also, the method workout the algebraic expression for relative velocities and volume fraction equation of the treated phases (Mishra et al., 2019).

Continuity Equation

The Eq. (8) describes the continuity expression for the phase mixture, given that, $\vec{u}_m$ is the averaged-mass velocity and ρ_m is the mixture density (Madhania et al., 2017).

$$\frac{\partial(\rho_m)}{\partial t} + \nabla.\left(\rho_m \vec{u}_m\right) = \dot{m} \tag{8}$$

$$\vec{u}_m = \frac{\sum_{k=1}^{n} \beta_k \rho_k \vec{u}_k}{\rho_m} \tag{8.1}$$

$$\rho_m = \sum_{k=1}^{n} \beta_k \rho_k \tag{8.2}$$

where $\dot{m}$ is the mass transferred as a result of cavitation formed, $\vec{u}_{dr,k}$ is the secondary phase drift velocity and β_k represent the volume fraction of any phase k.

The volume fraction equation from the continuity equation for the secondary phase p is provided in Eq. (9).

$$\frac{\partial(\rho_p \beta_p)}{\partial t} + \nabla \cdot \left(\beta_p \rho_p \vec{u}_m\right) = -\nabla \cdot \left(\beta_p \rho_p \vec{u}_{dr.p}\right) \tag{9}$$

Momentum Equation

With the mixture model, the overall momentum equation is derived by summing the individual phase momentum equation. The mixture momentum equation is therefore expressed as below (Madhania et al., 2017):

$$\frac{\partial\left(\rho_m \vec{u}_m\right)}{\partial t} + \nabla \cdot \left(\rho_m \vec{u}_m \vec{u}_m\right) = -\nabla p + \nabla \cdot \left[\mu_m \left(\nabla \vec{u}_m + \nabla \vec{u}_m^T\right)\right] + \rho_m \vec{g} + \vec{F} + \nabla \cdot \sum_{k=1}^{n} \beta_k \rho_k \vec{u}_{dr,k} \vec{u}_{dr,k} \tag{10}$$

where $\vec{F}$ is the body force, n represent the number of phases transported, and μ_m denote the viscosity of the mixture.

$$\mu_m = \sum_{k=1}^{n} \beta_k \mu_k \tag{10.1}$$

$$\vec{u}_{dr,k} = \vec{u}_k - \vec{u}_m \tag{10.2}$$

Energy Equation

As follows, the energy equation of the fixture is defined in Eq. (11). The variable k_{eff} is the effective conductivity of the mixture ($k+k_t$) which depends on the turbulent thermal conductivity value k_t, provided by the turbulence model implemented. The term $\nabla \cdot (k_{eff} \nabla T)$ is the heat transfer due to conduction and S_E takes into consideration any volumetric heat source introduced externally by the user (Mishra et al., 2019).

$$\frac{\partial}{\partial t} \sum_{k=1}^{n} (\beta_k \rho_k E_k) + \nabla \cdot \sum_{k=1}^{n} \beta_k \mu_k (\rho_k E_k - p) = \nabla \cdot (k_{eff} \nabla T) + S_E \tag{11}$$

The expression for the enthalpy of the phase k, (E_k) are of two types depending on the phase property. For incompressible phase, $E_k = h_k$, where h_k is the actual enthalpy of the phase k. For a compressible phase:

$$E_k = h_k - \frac{p}{\rho_k} + \frac{u_k^2}{2} \tag{11.1}$$

2.5.1. Surface tension and wall adhesion modelling

Generally, the Euler–Euler type of multiphase methods models the effect of surface tension at interfaces of contacting phases (continuous and discrete phase) (Vachaparambil and Einarsrud, 2019). Also, the model can be modified to specify contact angles between the walls and phases. With the mixture model, surface tension and wall adhesion modelling approach are very similar to each other (Liu and Luo, 2019).

Surface tension comes in-play because of attractive forces that exist between molecules in a fluid. However, IFT acts along interfaces of touching regions between fluids, and a solid. In Fluent, the continuum surface force (CSF) model along with the wall adhesion option is used for this purpose (Vachaparambil and Einarsrud, 2019). By activating this model, a source term containing the surface tension parameter is added to the momentum equation. To have a clear picture on the origin of the source term, assume a case where surface tension is constant throughout the flow field, and where only normal forces to the interface are considered (Vachaparambil and Einarsrud, 2019). Let σ describe the surface tension coefficient, r_1 and r_2 are the surface curvatures in orthogonal directions, we notice that pressure drop $(p_2 - p_1)$ is directly relate to σ. The relationship is communicated below. $p_2$andp_1 correspond to the pressure values two fluids at opposite sides of the interface (Liu and Luo, 2019).

$$p_2 - p_1 = \sigma\left(\frac{1}{r_1} + \frac{1}{r_2}\right) \tag{12}$$

In FLUENT, the local gradients along the surface normal to the interface is used to compute the surface curvature. The normal surface represented as n, is a function of the gradient of the volume fraction of the qth phase (Vachaparambil and Einarsrud, 2019).

$$n = \nabla\beta_q \tag{13}$$

The curvature constant term k, is defined by the unit normal divergence term $\hat{n} = \left(\frac{n}{|n|}\right)$.

$$k = \nabla\hat{n} \tag{14}$$

Herein, pressure projection across the surface serves as a metric to describe surface tension, numerically. The force term $\vec{F}$ in the Eq. (10) is technically expressed as volume force based on the divergence theorem. The volume force equation is provided in Eq. (15). Note that the computed volume force is less accurate in triangular and tetrahedral meshes as compared to quadrilateral and hexahedral meshes, since the volume-averaged density, ρ, is directly linked to the surface tension source term for a cell (Vachaparambil and Einarsrud, 2019). The cell size distribution affects the surface tension prediction. Therefore, domains discretized by equal cell sizes yields better accuracy (Liu and Luo, 2019).

$$\vec{F} = \sum_{pairsij,i<j} \sigma_{ij}\left[\frac{\alpha_i\rho_i k_j\nabla\alpha_j + \alpha_j\rho_j k_i\nabla\alpha_i}{\frac{1}{2}\left(\rho_i + \rho_j\right)}\right] \tag{15}$$

In the computational modelling, the surface tension effects are determined from the Reynolds number, R_e or Weber number, W_e and the capillary number C_a along the pore-throat. If $R_e = 1$, Eq. (16) can be used. However, $R_e \gg 1$, the Weber quantity is of interest. The expression is provided in Eq. (17) (Vachaparambil and Einarsrud, 2019).

$$C_a = \frac{\mu U}{\sigma} \tag{16}$$

$$W_e = \frac{\sigma}{\rho L U^2} \tag{17}$$

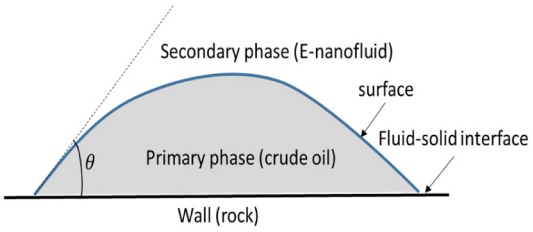

Fig. 4. Contact angle measurement in a computational cell.

Note that U is the free-stream velocity. Also, the surface effect is neglected in FLUENT, if $C_a \gg 1$ and $W_e \ll 1$.

Wall adhesion option available in FLUENT specifies wall adhesion angle along with the surface tension model. The contact angle made by the wall adjust the surface tension normal to the interface, instead of imposing a surface tension value in the boundary condition (Vachaparambil and Einarsrud, 2019). Eq. (18) is implemented numerically to achieve this such that θ_w is the contact angle, $\hat{t}_w$ and $\hat{n}_w$ are the unit vectors tangential and normal to the wall, respectively. The dynamic boundary condition creates adjustment of the curvature of the primary phase (crude oil) surface near the wall (Liu and Luo, 2019).

$$\hat{n} = \hat{n}_w cos\theta_w + \hat{t}_w sin\theta_w \tag{18}$$

Surface curvature is achieved in a cell through the inclusion of computed surface and angle the fluid makes with the wall surface. The local surface curvature adjusts the body force term during surface tension calculation. Fig. 4 is a diagrammatic representation of contact angle between the wall and the interface.

3. Results and discussion

3.1. Flow physics visualization

Herein, we modelled the fluid–solid interaction for the base case (without ethanol addition) using three different turbulence models independently as recorded in literature. The goal is to communicate the effectiveness of the chosen method (IDDES) with respect to its ability to resolve flow at steep curvatures near wall boundaries, where detached boarder-line flow prevail, and in areas with constant flow attachment. As seen in Fig. 5(a–b), flow propagation of the nanofluid with the unsteady RANS (URANS), hybrid RANS–LES (IDDES) and LES methods are presented for different periods, respectively.

We observe that all models are performing, however, the fluid track seems little exaggerated with the URANS approach in contrast to the IDDES and LES methods with hybrid RANS–LES method. LES approach has been proven more accurate than the RANS method. However, the LES method exhibits some weakness in simulating transitional turbulence flow near the wall boundaries depending upon the sub-grid scale model (see Guleren et al., 2010; Kahil et al., 2019). The RANS approach is most suitable in this region; however, less accurate solutions are obtained since large eddies containing the turbulent energy, responsible for momentum transfer and turbulent mixing are not considered. Instead, they are modelled with the RANS method unlike the LES approach that captures full details of this eddies. Consequently, turbulent flows involving separated shear layers cannot be accurately resolved with the RANS method. Hence, the hybrid RANS–LES (IDDES) model addresses the limitations of the individual methods, and combines their advantages making it suitable for this investigation where consistent separated shear layers and attached boundary layers flow is expected during the interactive

simulation run. Highlights of critical flow regions where flow detachment and attachment dominate are highlighted using break circles. The specific zones demonstrate that the hybrid method solves the turbulence closure problem quite well and properly resolves flow throughout the flow field. This way, we are able to mimic the actual flow behaviour of the interacting fluids under prescribed flow media characteristics.

3.2. Base case CFD analysis

The ability for the flooded fluid to make good association with crude oil subsurface, and to improve the mobility of the contacted fluid is termed sweep efficiency (SE) or displacement efficiency (DE). Note that the greater the SE, the higher the reservoir performance and economic viability of the exploration and production project. Herein, the base fluid (silica nanofluid) is introduced at a constant velocity of 1 m/s through the inlet section where pressure is at its maximum level, and modelled to interact or slip instantaneously with nearby no-flow boundaries. The flow rate of the introduced solution is made consistent to supplement kinetic energy lost by the secondary phase as it makes contact and mobilizes the primary phase. The absorbed energy causes the primary to gain momentum and propagate towards the low-pressure zone (outlet). However, due to the heterogeneous nature of the flow field, the fluids velocity and pressure are unevenly distributed thereby engendering effective oil recovery, which is inevitable in real-life cases. Areas characterized with high flow properties experience higher DE of the primary phase and vice versa. Fig. 6(a) shows a clear demonstration of crude oil volume ratio as the pressurized nanofluid produced during flow for different periods t. At $t = 75$ s, we see that the injected fluid has travelled virtually half the entire 60 m lateral length of the flow section, which give us a fair idea about the pressure exerted at the fluid's contact front. However, it is perceived using the colour code that, about 53% of the primary phase volume is displaced, leaving about 47% of the primary phase initial volume behind. One could say that, viscous fingering may have occurred due to viscosity difference or inability for the injected fluid to chemically and/or mechanically interact with the primary fluid. Hence, greater tendency to override the primary phase bank due to gravity effect. Note that, the red colour represents un-displaced crude oil, and green denote areas flushed by the injected fluid. Effective displacement of the primary phase relies strongly upon the ability for the injected fluid to overcome the attractive force binding or holding the primary phase attached the wall surface tension. Recall that the surface tension between the wall and primary phase is at its maximum (> 0.038). As discussed previously, the chemical reaction kinetics module in ANSYS is responsible for modelling chemical reaction occurring at all interfaces during simulation. That way, reduction in the surface forces contributed to increase in velocity of the primary phase from $u_i = 0$ m/s to $v = u_{i+1}$, where i is the position and $u_{i+1} \neq 0$ is the predicted velocity at node i; the same applies to other spatial directions, and static pressure. Contour plots describing the velocity of the mixture is revealed in Fig. 7(a)–(d), respectively.

3.3. Effect of adding ethanol

Ethanol is widely known to have good interfacial properties for cleaning oil-stains, besides its current use as renewable energy source for powering automotive engines. Wouters et al. (2017) found that gluten hydrolysates instituted very weak interfacial films in the presence of ethanol, and the same applied to reduction in air–water surface tension. Compared to nanoparticles in the solution state, ethanol possesses higher tendency to form strong covalent bonds with hydrocarbons. Consequently, the bonding transforms the viscous and dense hydrocarbon compound to a lighter form dominated with single hydrogen bonds. Technically, the oil is metamorphosed from dead to live (less dense and mobile oil). Herein, we attempt to numerically study the impact on ethanol addition in different proportions to oil's DE. A blend of 30% ethanol and 70% base fluid is modelled using the mixture model to form E-N-30, and further addition of 20% ethanol (E-N-30) is fashioned computation-wise.

Initial introduction of E-N-30 blend contributed to a further 39% (estimated sum of 92%) displacement in crude oil's volume fraction as expressed in Fig. 6(b) within the same time frame as the base case. Utilizing the colour codes, we discover that the transmission media is more bluish indicating high sweeping performance of the blend. However, we discover that the travel distance is much smaller relative to that obtained with the base fluid under same periods. It can be inferred that; higher retention time is spotted with the second injection case. In connection to this, we have numerically proven that the chemical kinetics at mesh scale favours E-N-30 fluid in terms of conquering the oil–wall binding force. Furthermore, we notice velocity and pressure distribution enhancement throughout the flow domain in Fig. 7(c)–(d), respectively, which accounted for the success of E-N-30 fluid. The numerical outcome is verified experimentally. Further discussion on this is provided in subsequent section.

3.4. Experimental validation of CFD model

A simple experiment conducted by Dr. Eric Branson at the University of Mines and Technology, Ghana petroleum-engineering laboratory to validate the hypothesis made in this paper concerning the interfacial properties of biofuels in general. A 0.5 ml cylindrical container was partially filled with a mixture of sand, water and crude oil for the base case, and the biofuel was added later to form the after-case. The main idea was to wet the sand particles with oil to mimic oil-wetting sandstone formations. Afterwards, the biofuel is introduced into the mixture to study the freed-surface flow by flipping the container downwards. From critical look of Fig. 8(a), we notice that the immediate layer below the container's uppermost boundary and above the mixture height is stained with oil–sand indicating high interfacial/molecular attraction between the mixture and bottle surface. On adding the biofuel roughly about 30% and flipped downwards, we perceive that the oil–sand stain is almost cleaned off such that the we can see through the bottle. However, the upmost part of the container as shown in Fig. 8(b) imbibes an accumulation of the mixture. Here, we propose that the mixture was not well shaken to create minimize non-uniformity of the mixture. In summary, the experimental demonstration has established strong evidence to back our hypothesis on the potential for biofuels, especially ethanol to significantly reduce interfacial tension. A visual of experimental results is displayed in Fig. 8.

3.5. Sensitivity analysis

Herein, we are determined to study the effect of adding different proportions of the biofuel to oil recovery measured at the outlet boundary based on the flow rate, a function of the volume of crude oil displaced for every time step. The analysis is performed for the blend cases: E-N-0 (0% ethanol), E-N-30 (30% ethanol) and E-N-50 (50% ethanol). The impact of porosity and injection rate are out of research scope due to the fact that, it has been well established that the more compacted the formation becomes, the higher the flow rate, and this follows the basic principle of squeezing liquid out of foamy material. Three nanofluids are considered, and reasons behind the choice was mentioned in Section 2.3. The analysis is applicable for all three

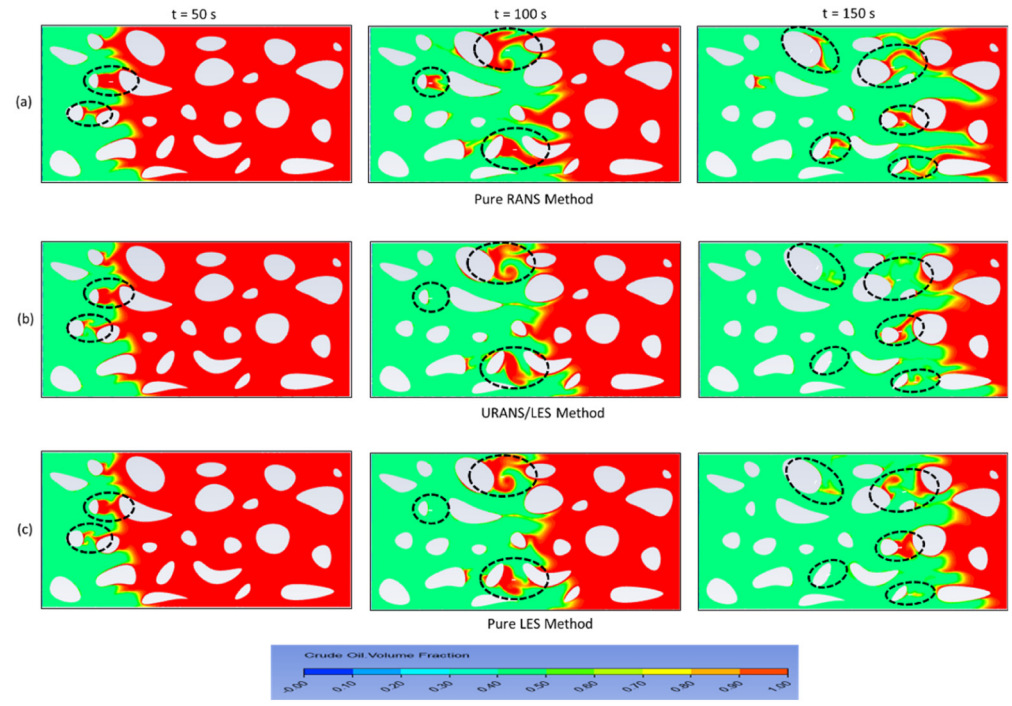

Fig. 5. Flow visualization of nanofluid infusion through porous media using (a) pure RANS method, (b) hybrid RANS–LES method, and (c) pure LES method.

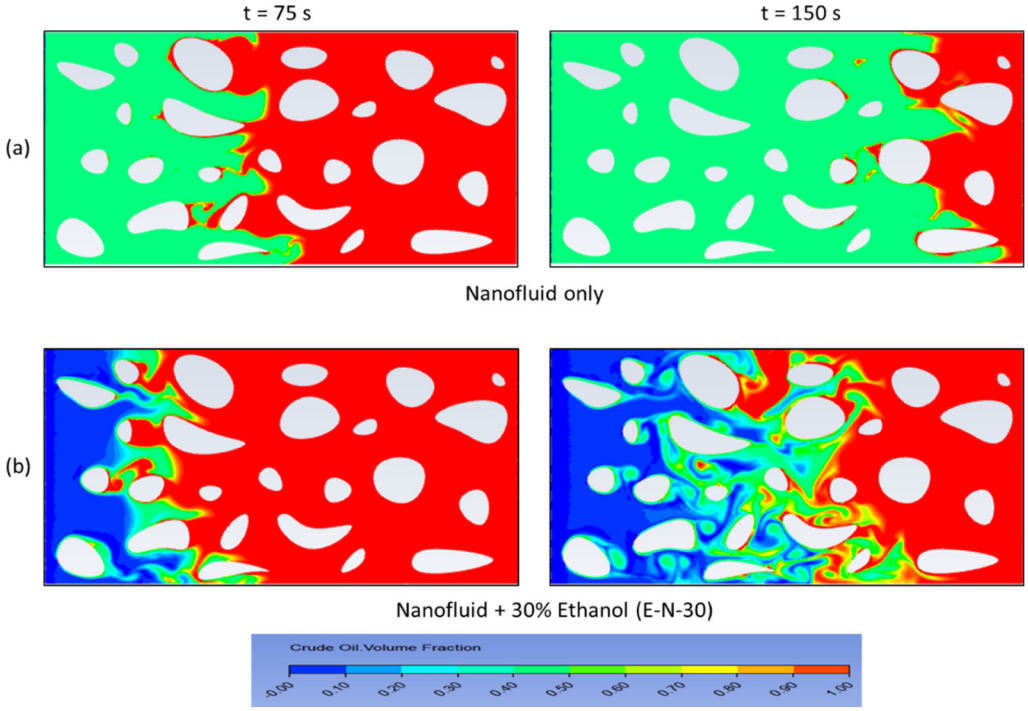

Fig. 6. Crude oil volume ratio contour plot showing DE of the nanofluid (a) without and (b) with, the addition of ethanol chemical.

base fluids. In addition, ethanol is introduced at the same rate with the base fluid to model the impression that both fluids flow as one, such that the mixture model takes care of assigning the volume fraction of each injected phases at the inlet boundary. The simulation is performed for a period of 200 s, and the objective results are plotted as shown in Fig. 9. Fig. 9(a)–(c) delineate the oil recovery profile for E-N-0, E-N-30 and E-N-50 blends, respectively. It is noticed that the crude oil's flow rate profile is unsteady depicting non-homogeneity of the flow trajectory. Furthermore, the number of amplitude wave length after a specific period communicate the degree of heterogeneity or Petrophysical state of the reservoir in terms of rock and fluid properties. However, optimal reservoir performance can only be achieved for uniformly distributed Petrophysical formation characteristics.

Technically, improvements in the flow rate of a fluid relative to the other in a typical multiphase flow system, gives a clear or broader view on the reduced effect of IFT. In petroleum reservoirs, the formation of emulsion between the immiscible fluids (oil

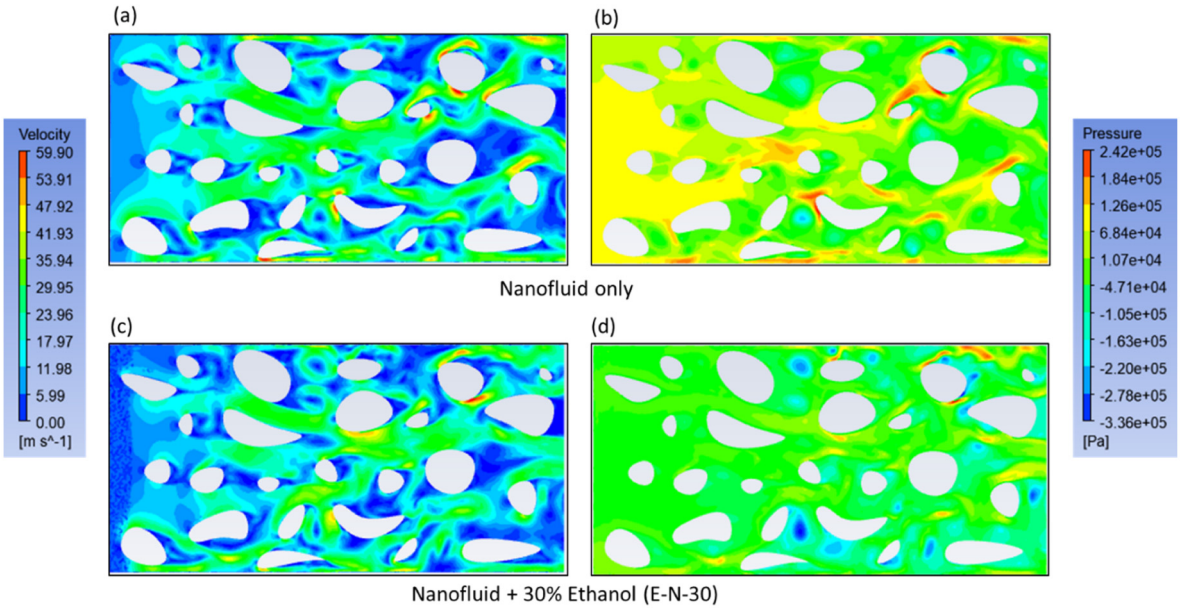

Fig. 7. Velocity magnitude and mixture pressure contour plot for the flowing nanofluid-blend.

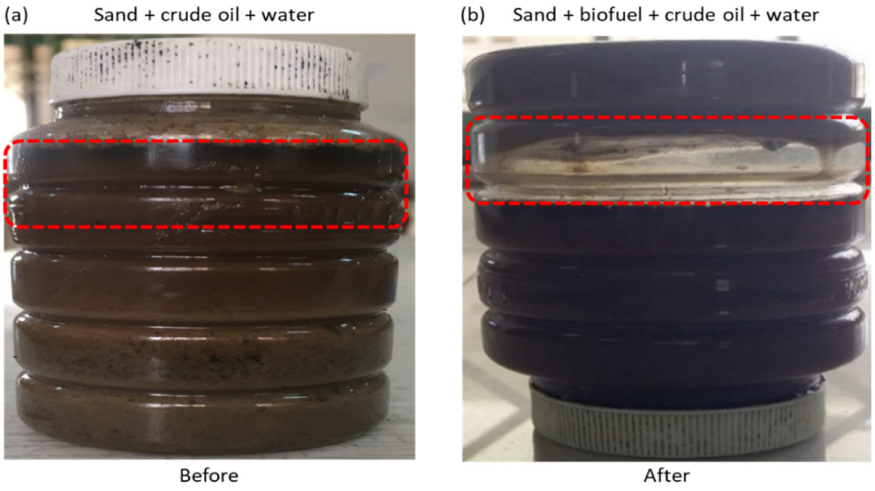

Fig. 8. Image revealing cleaning of oil–sand stain with biofuel in a 0.5 ml container.

and water) is the major cause for low oil relative permeability. Relative permeability is a function of the ease for a fluid to flow relative to the other interacting phases. It implies that the effect of reduced IFT can be interpreted in terms of relative permeability or flow rate. In this paper, we chose measure the effect of IFT reduction through the flow efficiency of the target fluid. This a way, a 10% increase in flow rate is translated to a 10% decrease in IFT and so forth. Contrasting the production profiles for all cases, we observe that on subsequent addition of ethanol up to 50%, the flow rate data with silicon carbide nanofluid blend becomes very distinct compared to the other two cases with relatively higher average flow rate. Moreover, the blend cases with silica nanofluid are perceived to perform optimally throughout, making it the best choice for EOR process. The hypothesis is confirmed from experimental findings revealed in Roustaei et al. (2012), Ogolo et al. (2012), Esfandyari Bayat et al. (2014), Roustaei and Bagherzadeh (2015), Nazari Moghaddam et al. (2015), Sun et al. (2017), Ding et al. (2019), Afekare et al. (2020), Esfe et al. (2020) and Qin et al. (2020) research. Once again, the agreement confirms the usefulness and efficiency of numerical models to address real-world engineering challenges. At the end of flow period, about 46.34% of residual volumes of crude oil left behind after injecting the base fluid, indicated in Fig. 9(d). It should be noted that the superior interfacial, thermal and mechanical properties of silica nanoparticle (Table 2) compared to its counterpart played a remarkable role in its success.

3.6. Effect of temperature to DE

In the previous section, it was realised that, peak recovery efficiency is achievable using silica nanofluid blend. However, the flow was modelled at ambient condition. Herein, the energy equation is activated numerically to study the influence of temperature to the performance of the optimal chemical formulation to make critical decision on the thermal stability of the blend. By activating the energy equation enables dynamic computation of the phase viscosity based on the kinetic theory. The domain temperature θ is elevated from 298 K to 400 k, to imitate typical petroleum reservoir temperatures. According to Gay-Lussac's Law, temperature and pressure vary proportional to each other at constant volume. This principle is numerically implemented in this work through the activation of the energy

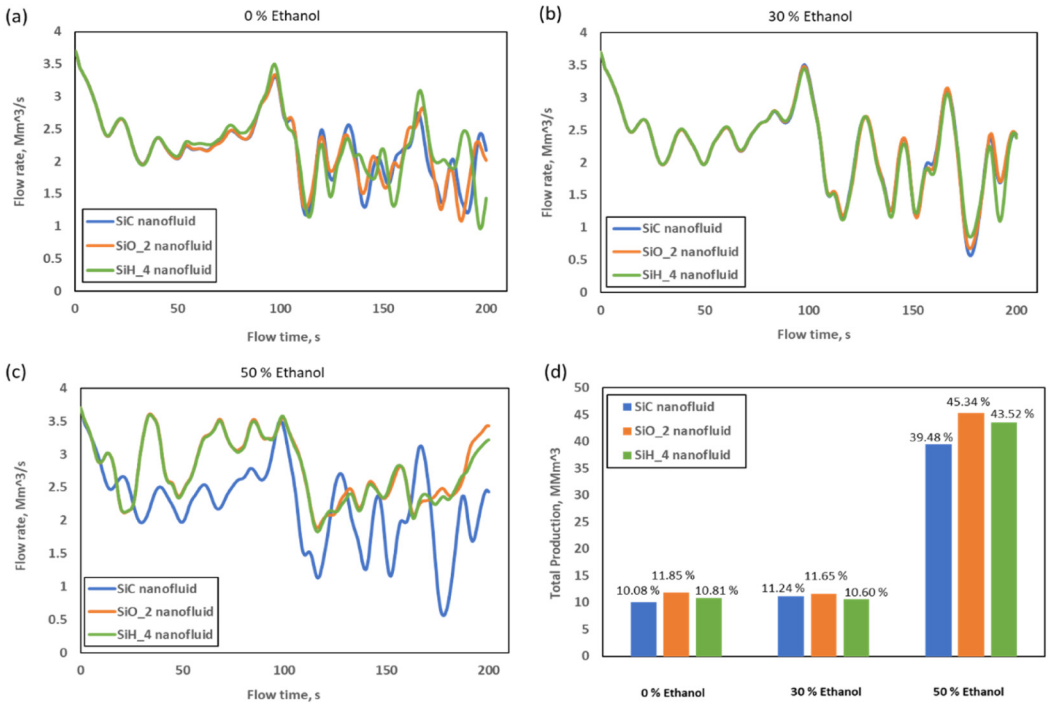

Fig. 9. Residual crude oil flow rate plot for (a) 0% Ethanol addition, (b) 30% Ethanol addition, (c) 50% Ethanol addition and (d) comparative total production plot, with silicon-based nanofluid injection.

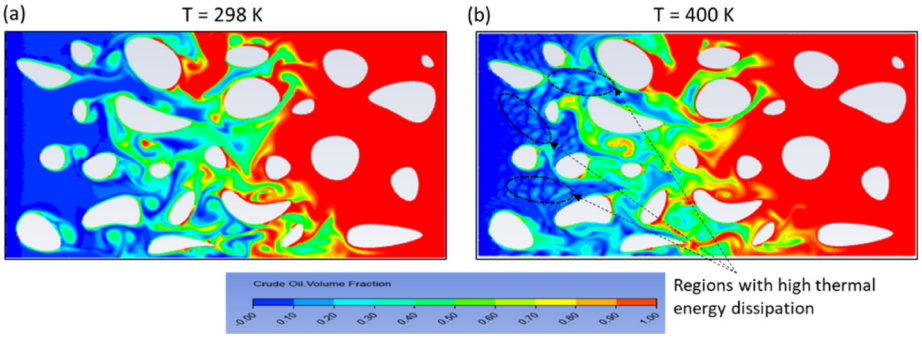

Fig. 10. Flow visualization of crude oil volume ratio at temperatures (a) 298 K and (b) 400 K.

equation. Moreover, when the temperature of the reacting region is increased, gross fluidic molecular instability is experienced, which led to high kinetic energy dissipation. The thermal interaction accounts for the instabilities in the flow features highlighted with dotted circles in Fig. 10. The crude oil volume fraction contour plot at $\theta = 298$K and $\theta = 400$K are provided in Fig. 10(a) and Fig. 10(b), respectively.

At high temperatures, the formation of wavy features within the flushed zones is perceived. Here, the thermal resilience of the proposed blend is tested for their volumetric flow performance. The corresponding volumetric plots are shown in Fig. 11. Notably, the blend performance at $\theta = 400$ K outweighed that at $\theta = 298$ K, irrespective of the volatile nature or low thermal conductivity of ethanol. Also, an increase in the oil's flow rate of about 16.1 Mm^3/s is achieved, and this contributed to approximately 60.24% increase in oil production rate when compared to the base case. It shoul be noted that, silica nanoparticles possess excellent thermal stability. As a result, their presence in the mixture considerably assisted to retain state of the blend. Furthermore, an increase in temperature enhanced the chemical reactivity interacting phases, and also plays a noteworthy role in weakening the interfacial forces and distabilizes possible presence of emulsion that prevents flow of a particular phase.

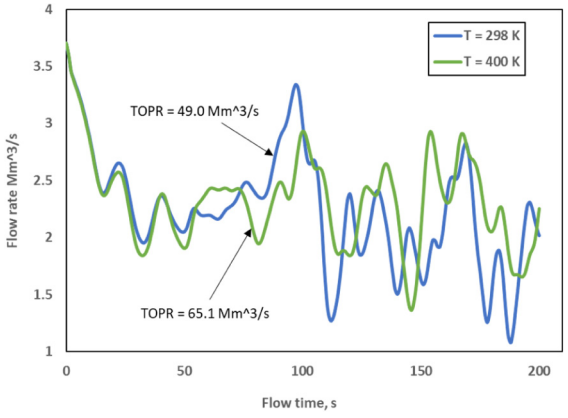

Fig. 11. Plot of volumetric flow rate against time for different flow conditions.

4. Conclusions

In this paper, the major concerns faced by the petroleum industry with regards to optimizing the performance of enhanced oil recovery (EOR) chemicals has been addressed through the implementation of advanced numerical transport and energy equations. Impulsive emulsion formation, porous media wettability alteration, and interfacial tension (IFT) reduction are a list of advantages that could be derived from the effective use of nanoparticles for EOR purpose due to their potential to create high disjoining pressure near the fluid–rock interface. Furthermore, low sweep efficiency (SE) resulting from poor mixing of the injected nanofluid while redeeming the immobile volume of crude oil subsurface can become a major factor. In this paper, the influence of ethanol to IFT reduction and dead oil displacement efficiency when blended with nanofluids was studied numerically. The amalgamation of ethanol and the various types of silicon-based nanofluids were modelled using the mixture model. Amongst the three commonly used silicon-based nanofluid applied to enhance the functionality of engineering materials, silica nanofluid proved to out-weigh the others interms of sweep efficiency. Moreover, its performance was significantly improved when combined with ethanol at equal proportions. The increase in the recovery of the primary phase is a clear reflection of the performance improvement. The effective interfacial and chemical properties of ethanol stimulated superior mixing and displacement of the primary phase by reducing the IFT restraining the crude oil to the grain wall surface. This propelled the originally trapped oil forward with a relatively lower viscosity/density. From chemical reaction point-of-view, water molecules are produced from the reaction, most of which settles at the fluid-solid interfaces to alter the wettability of the solid surface from oil-wet to water-wet. However, the amount of water concentration generated is out of the research scope. Furthermore, the domain temperature was attenuated from ambient condition 298.15 K to 400 K to replicate conditions similar to those observed in actual petroleum reservoirs. Conclusively, an additional 55.34% of the dead oil volume is displaced using the optimal blend formulation. However, this recovery factor may not be equal as those obtained from a typical field test due to certain dynamic attributes of petroleum reservoirs that is difficult to replicate or capture through numerical modeling. Moreover, the obtained recovery efficiency from the numerical study gives the reader a good indication of the expected success of the proposed blend for EOR projects, and an estimate of the incremental recovery efficiency of the initially leftover oil, if implemented. Nevertheless, an experiment was carried-out using sand particles, oil, water and biofuel to verify the research hypothesis. The inclusion of biofuel was found to effectively clean the oil-stains on the walls of the container, making the flushed surface less oil-wetting.

CRediT authorship contribution statement

Chukwugozie Ejeh: Conceived and designed the experiment, Perform the experiment and wrote the paper. **Imran Afgan:** Conceived, wrote and reviewed the paper, Supported provided to reagents. **Hamzah AlMansob:** Provided reagents. **Eric Brantson:** Wrote the paper, Performed the experiment and contributed reagents. **Joseph Fekala:** Contributed reagents. **Micah Odiator:** Contributed reagents. **Promise Stanley:** Contributed reagents. **Prosper Anumah:** Contributed reagents. **Chigozirim Onyekperem:** Contributed reagents. **Evans Boah:** Contributed reagents.

Declaration of competing interest

The authors declare that they have no known competing financial interests or personal relationships that could have appeared to influence the work reported in this paper.

Acknowledgment

The authors would like to thank Khalifa University Abu Dhabi for providing the necessary facilities and acknowledge the funding provided through ADERP grant 8474000240 (FSU-2020-16).

References

Abed, N., Afgan, I., 2019. Enhancement techniques of parabolic trough collectors: A review of past and recent technologies. Adv. Civ. Eng. Tech. 33, 313–318.

Abed, N., Afgan, I., 2020. An extensive review of various technologies for enhancing the thermal and optical performances of parabolic trough collectors. Int. J. Energy Res. 44, 5117–5164.

Abed, N., Afgan, I., Iacovides, H., Cioncolini, A., Nasser, A., 2020. Assessment and evaluation of the thermal performance of various working fluids in parabolic trough collectors of solar thermal power plants under non-uniform heat flux distribution conditions. Energies 13 (15), 3778.

Afekare, D., Gupta, I., Rao, D., 2020. Nanoscale investigation of silicon dioxide nanofluids and implications for enhanced oil recovery–an atomic force microscope study. J. Pet. Sci. Eng. 191, 107165;
Belyadi, H., Fathi, E., Belyadi, F., 2019. Hydraulic Fracturing in Unconventional Reservoirs: Theories, Operations, and Economic Analysis. Gulf Professional Publishing.

Ahmed, U., Apsley, D., Stallard, T., Stansby, P., Afgan, I., 2020. Turbulent length scales and budgets of Reynolds stress-transport for open-channel flows; friction Reynolds numbers (Re_τ)= 150, 400 and 1020. J. Hydraul. Res. 1–15.

Al-Anssari, S., Barifcani, A., Wang, S., Maxim, L., Iglauer, S., 2016. Wettability alteration of oil-wet carbonate by silica nanofluid. J. Colloid Interface Sci. 461, 435–442.

Al-Maskari, N.S., Saeedi, A., Xie, Q., 2019. Alcohol-assisted waterflooding in carbonate reservoirs. Energy Fuels 33 (11), 10651–10658.

Al-Murayri, M.T., Hassan, A.A., Abdullah, M.B., Abdulrahim, A.M., Marlière, C., Hocine, S., Tabary, R., Suzanne, G.P., 2019. Surfactant/polymer flooding: Chemical-formulation design and evaluation for raudhatain lower burgan reservoir Kuwait. SPE Reserv. Eval. Eng. 22 (03), 923–940.

Alam, M.F., Thompson, D., Walters, D.K., 2017. Critical assessment of hybrid RANS-LES modelling for attached and separated flows. In: Turbulence Modelling Approaches: Current State, Development Prospects, Applications. p. 1.

Benhamadouche, S., Afgan, I., Manceau, R., 2019. Numerical simulations of flow and heat transfer in a wall-bounded pin matrix. Flow Turbul. Combust. 104, 19–44.

Boah, E.A., Kondo, O.K.S., Borsah, A.A., Brantson, E.T., 2019. Critical evaluation of infill well placement and optimization of well spacing using the particle swarm algorithm. Journal of Petroleum Exploration and Production Technology 9 (4), 3113–3133.

Delafin, P.L., Nishino, T., Kolios, A., Wang, L., 2017. Comparison of low-order aerodynamic models and RANS CFD for full-scale 3D vertical axis wind turbines. Renew. Energy 109, 564–575.

Ding, H., Zhang, N., Zhang, Y., Wei, M., Bai, B., 2019. Experimental data analysis of nanoparticles for enhanced oil recovery. Ind. Eng. Chem. Res. 58 (27), 12438–12450.

Druetta, P.D., 2019. Numerical modelling of nanotechnology-boosted chemical enhanced oil recovery methods. In: Computational Fluid Dynamics Simulations. IntechOpen.

Ejeh, C., Afgan, I., Shittu, R., Sakirudeen, A., Anumah, P., 2020a. Investigating the impact of velocity fluctuations and compressibility to aerodynamic efficiency of a fixed-wing aircraft. Results Phys. 103263.

Ejeh, C.J., Akhabue, G.P., Agyeibi, I., 2019. Effect of transient temperature on 304 stainless steel LPG tank structure using numerical simulation approach. SN Appl. Sci. 1 (12), 1690.

Ejeh, C.J., Barsoum, I., Chizindu, G.O., Kodie, G.M., Anachuna, J.I., 2020b. Thermo-elastic behaviour of carbon-fiber reinforced polymer and the effect of adding nanoparticles at elevated heat intensity. Heliyon 6 (3), e03622.

Ejeh, C.J., Boah, E.A., Akhabue, G.P., Onyekperem, C.C., Anachuna, J.I., Agyebi, I., 2020c. Computational fluid dynamic analysis for investigating the influence of pipe curvature on erosion rate prediction during crude oil production. Exp. Comput. Multiph. Flow 2 (4), 255–272.

Ejeh, C.J., Mawufemor, G.P.H., Ransford, A., 2020d. Sulfolane and di-iso-propanol lean amine blend operating temperature and pressure effect to natural gas sweetening using process simulation. SN Appl. Sci. 2 (2), 295.

El-Diasty, A.I., Aly, A.M., 2015. Understanding the mechanism of nanoparticles applications in enhanced oil recovery. In: SPE North Africa Technical Conference and Exhibition. Society of Petroleum Engineers, September.

Esfandyari Bayat, A., Junin, R., Samsuri, A., Piroozian, A., Hokmabadi, M., 2014. Impact of metal oxide nanoparticles on enhanced oil recovery from limestone media at several temperatures. Energy Fuels 28 (10), 6255–6266.
Esfe, M.H., Esfandeh, S., Hosseinizadeh, E., 2020. Nanofluid flooding for enhanced oil recovery in a heterogeneous two-dimensional anticline geometry. Int. Commun. Heat Mass Transfer 118, 104810.
Fard, A.K., Rhadfi, T., Mckay, G., Al-marri, M., Abdala, A., Hilal, N., Hussien, M.A., 2016. Enhancing oil removal from water using ferric oxide nanoparticles doped carbon nanotubes adsorbents. Chem. Eng. J. 293, 90–101.
Fereidooni Moghadam, T., Azizian, S., 2014. Effect of ZnO nanoparticle and hexadecyltrimethylammonium bromide on the dynamic and equilibrium oil–water interfacial tension. J. Phys. Chem. B 118 (6), 1527–1534.
Ferreira, A.C., Sullo, A., Winston, S., Norton, I.T., Norton-Welch, A.B., 2020. Influence of Ethanol on emulsions stabilized by low molecular weight surfactants. J. Food Sci. 85 (1), 28–35, swx.
Filippone, A., Afgan, I., 2008. Orthogonal blade-vortex interaction on a helicopter tail rotor. AIAA J. 46 (6–1476).
Gharibshahi, R., Jafari, A., Ahmadi, H., 2019. CFD Investigation of enhanced extra-heavy oil recovery using metallic nanoparticles/steam injection in a micromodel with random pore distribution. J Pet. Sci. Eng. 174 (374–383).
Giraldo, J., Benjumea, P., Lopera, S., Cortés, F.B., Ruiz, M.A., 2013. Wettability alteration of sandstone cores by alumina-based nanofluids. Energy Fuels 27 (7), 3659–3665.
Guleren, K.M., Afgan, I., Turan, A., 2010. Predictions of turbulent flow for the impeller of a NASA low-speed centrifugal compressor. J. Turbomach. Trans. ASME 132 (2-21005).
Huang, B., Hu, X., Fu, C., Zhou, Q., 2020. Experimental study on the effect of ASP flooding on improving oil recovery in low permeability reservoirs based on a partial quality tool. Processes 8 (3), 296.
Jafari, A., Hasani, M., Hosseini, M., Gharibshahi, R., 2019. Application of CFD technique to simulate enhanced oil recovery processes: current status and future opportunities. Pet. Sci. 1–23.
Jamal, T., Wang, H., Walters, D.K., 2018. LES And hybrid RANS-LES simulation of a pulsating channel flow. In: ASME 2018 International Mechanical Engineering Congress and Exposition. American Society of Mechanical Engineers Digital Collection.
Jekwu, E.C., 2018. Numerical simulation on the impact of polymer salt concentration to Alkaline-Surfactant-Polymer flooding. Thought 6 (1), 191–220.
Ju, B., Fan, T., 2009. Experimental study and mathematical model of nanoparticle transport in porous media. Powder Technol. 192 (2), 195–202.
Kahil, Y., Benhamadouche, S., Berrouk, A.S., Afgan, I., 2019. Simulation of subcritical-Reynolds-number flow around four cylinders in square arrangement configuration using LES. J. Mech. B/Fluids 74, 111–122.
Kazemzadeh, Y., Shojaei, S., Riazi, M., Sharifi, M., 2019. Review on application of nanoparticles for EOR purposes: A critical review of the opportunities and challenges. Chin. J. Chem. Eng. 27 (2), 237–246.
Kim, M., Haroun, M., Rahman, M.M., Kobaisi, M.A., 2019. Hybrid nano acid fluid pulsed with electrokinetic to stimulate tight carbonate reservoirs: A novel EOR/IOR method. In: SPE/IATMI Asia Pacific Oil & Gas Conference and Exhibition. Society of Petroleum Engineers, October.
Li, S., Ge, Y., Shi, Y., 2019. An iterative dynamic programming optimization based on biorthogonal spatial–temporal hammerstein modelling for the enhanced oil recovery of ASP flooding. J. Process Control 73, 75–88.
Lilly, D.K., 1992. A proposed modification of the Germano subgrid-scale closure method. Phys. Fluids A 4 (3), 633–635.
Liu, Q., Luo, Z., 2019. Modelling bubble column reactor with the volume of fluid approach: Comparison of surface tension models. Chin. J. Chem. Eng.
Madhania, S., Nurtono, T., Cahyani, A.B., Muharam, Y., Winardi, S., Purwanto, W.W., 2017. Mixing behaviour of miscible liquid-liquid multiphase flow in stirred tank with different marine propeller installment by computational fluid dynamics method. Chem. Eng. Trans. 56, 1057–1062.
Mishra, S., Misra, A., Rao, P.R., Rao, D.N., 2019. Multiphase mixture model simulation over a simplified car.
Nazari Moghaddam, R., Bahramian, A., Fakhroueian, Z., Karimi, A., Arya, S., 2015. Comparative study of using nanoparticles for enhanced oil recovery: wettability alteration of carbonate rocks. Energy Fuels 29 (4), 2111–2119.
Nguyen, P.T., Uribe, J.C., Afgan, I., Laurence, D.R., 2019. A dual-grid hybrid RANS/LES model for under-resolved near-wall regions and its application to heated and separating flows. Flow Turbul. Combust. 1–25.
Norton, T., Sun, D.W., 2006. Computational fluid dynamics (CFD)–an effective and efficient design and analysis tool for the food industry: a review. Trends Food Sci. Technol. 17 (11), 600–620.
Ogolo, N.A., Olafuyi, O.A., Onyekonwu, M.O., 2012. Enhanced oil recovery using nanoparticles. In: SPE Saudi Arabia Section Technical Symposium and Exhibition. Society of Petroleum Engineers, January.
Onyekonwu, M.O., Ogolo, N.A., 2010. Investigating the use of nanoparticles in enhancing oil recovery. In: Nigeria Annual International Conference and Exhibition. Society of Petroleum Engineers, January.
Pal, S., Mushtaq, M., Banat, F., Al Sumaiti, A.M., 2018. Review of surfactant-assisted chemical enhanced oil recovery for carbonate reservoirs: challenges and future perspectives. Pet. Sci. 15 (1), 77–102.
Paterson, E.G., Peltier, L.J., 2005. Detached-eddy simulation of high-Reynolds-number beveled-trailing-edge boundary layers and wakes.
Phukan, R., Gogoi, S.B., Tiwari, P., 2019. Enhanced oil recovery by alkaline-surfactant-alternated-gas/CO_2 flooding. J. Pet. Explor. Prod. Technol. 9 (1), 247–260.
Qin, T., Goual, L., Piri, M., Hu, Z., Wen, D., 2020. Nanoparticle-stabilized microemulsions for enhanced oil recovery from heterogeneous rocks. Fuel 274, 117830.
Revell, A., Afgan, I., Ali, A., Santasmasas, M., Craft, T., de Rosis, A., Holgate, J., Laurence, D., Iyamabo, B., Mole, A., Owen, B., 2020. Coupled hybrid RANS-LES research at the university of manchester. ERCOFTAC Bull. 120, 67.
Rezaei, A., Riazi, M., Escrochi, M., Elhaei, R., 2020. Integrating surfactant, alkali and nano-fluid flooding for enhanced oil recovery: A mechanistic experimental study of novel chemical combinations. J. Molecular Liquids 113106.
Rezaeiha, A., Montazeri, H., Blocken, B., 2019. CFD Analysis of dynamic stall on vertical axis wind turbines using Scale-Adaptive Simulation (SAS): Comparison against URANS and hybrid RANS/LES. Energy Convers. Manage. 196, 1282–1298.
Rostami, P., Sharifi, M., Aminshahidy, B., Fahimpour, J., 2019. The effect of nanoparticles on wettability alteration for enhanced oil recovery: micromodel experimental studies and CFD simulation. Pet. Sci. 16 (4), 859–873.
Roustaei, A., Bagherzadeh, H., 2015. Experimental investigation of SiO_2 nanoparticles on enhanced oil recovery of carbonate reservoirs. J. Pet. Explor. Prod. Technol. 5 (1), 27–33.
Roustaei, A., Moghadasi, J., Bagherzadeh, H., Shahrabadi, A., 2012. An experimental investigation of polysilicon nanoparticles' recovery efficiencies through changes in interfacial tension and wettability alteration. In: SPE International Oilfield Nanotechnology Conference and Exhibition. Society of Petroleum Engineers, January.
Safaei, A., Esmaeilzadeh, F., Sardarian, A., Mousavi, S.M., Wang, X., 2020. Experimental investigation of wettability alteration of carbonate gas-condensate reservoirs from oil-wetting to gas-wetting using Fe_3O_4 nanoparticles coated with poly (vinyl alcohol), (PVA) or hydroxyapatite (HAp). J. Pet. Sci. Eng. 184, 106530.
Shedid, S.A., 2015. Experimental investigation of alkaline/surfactant/polymer (ASP) flooding in low permeability heterogeneous carbonate reservoirs. In: SPE North Africa Technical Conference and Exhibition. Society of Petroleum Engineers, September.
Sheng, J.J., 2010. Modern Chemical Enhanced Oil Recovery: Theory and Practice. Gulf Professional Publishing.
Sheng, J.J., 2013. Enhanced Oil Recovery Field Case Studies. Gulf Professional Publishing.
Shobayo, O.O., Walters, D.K., 2018. Evaluation of performance and code-to-code variation of a dynamic hybrid RANS/LES model for simulation of backward-facing step flow. In: ASME 2018 5th Joint US-European Fluids Engineering Division Summer Meeting. American Society of Mechanical Engineers Digital Collection.
Shur, M.L., Spalart, P.R., Strelets, M.K., Travin, A.K., 2008. A hybrid RANS-LES approach with delayed-DES and wall-modelled LES capabilities. Int. J. Heat Fluid Flow 29 (6), 1638–1649.
Spalart, P.R., Deck, S., Shur, M.L., Squires, K.D., Strelets, M.K., Travin, A., 2006. A new version of detached-eddy simulation, resistant to ambiguous grid densities. Theor. Comput. Fluid Dyn. 20 (3), 181.
Suleimanov, B.A., Ismailov, F.S., Veliyev, E.F., 2011. Nanofluid for enhanced oil recovery. J. Pet. Sci. Eng. 78 (2), 431–437.
Sun, C., Guo, H., Li, Y., Jiang, G., Ma, R., 2020. Alkali effect on alkali-surfactant-polymer (ASP) flooding enhanced oil recovery performance: Two large-scale field tests' evidence. J. Chem. 2020.
Sun, X., Zhang, Y., Chen, G., Gai, Z., 2017. Application of nanoparticles in enhanced oil recovery: a critical review of recent progress. Energies 10 (3), 345.
Vachaparambil, K.J., Einarsrud, K.E., 2019. Comparison of surface tension models for the volume of fluid method. Processes 7 (8), 542.
Van Hooff, T., Blocken, B., Tominaga, Y., 2017. On the accuracy of CFD simulations of cross-ventilation flows for a generic isolated building: comparison of RANS, LES and experiments. Build. Environ. 114, 148–165.
Wouters, A.G., Rombouts, I., Fierens, E., Brijs, K., Blecker, C., Delcour, J.A., 2017. Impact of ethanol on the air-water interfacial properties of enzymatically hydrolyzed wheat gluten. Colloids Surf. A 529, 659–667.
Wu, Z., Laurence, D., Afgan, I., 2017a. Direct numerical simulation of a low momentum round jet in channel crossflow. Nucl. Eng. Des. 313, 273–284.

Wu, Z., Laurence, D., Iacovides, H., Afgan, I., 2017b. Direct simulation of conjugate heat transfer of jet in channel crossflow. Int. J. Heat Mass Transfer 110 (193–208), 193–208.
Wu, Z., Laurence, D., Utyuzhnikov, S., Afgan, I., 2019. Proper orthogonal decomposition and dynamic mode decomposition of jet in channel crossflow. Nucl. Eng. Des. 344, 54–68.
Xu, K., Ruan, B., Meng, H., 2018. Validation and analyses of RANS CFD models for turbulent heat transfer of hydrocarbon fuels at supercritical pressures. Int. J. Therm. Sci. 124, 212–226.
Yang, P., Li, Z.A., Xia, B., Yuan, Y.J., Huang, Q.T., Liu, W.L., Cheng, C.Y., 2019. Comprehensive review of alkaline–surfactant–polymer (ASP)-enhanced oil recovery (EOR). In: Proceedings of the International Field Exploration and Development Conference 2017. Springer, Singapore, pp. 858–872.
Youssif, M.I., El-Maghraby, R.M., Saleh, S.M., Elgibaly, A., 2018. Silica nanofluid flooding for enhanced oil recovery in sandstone rocks. Egypt. J. Pet. 27 (1), 105–110.
Zhang, L., Liu, P., Wang, T., 2011. Preparation of superparamagnetic polyaniline hybrid hollow microspheres in oil/water emulsion with magnetic nanoparticles as cosurfactant. Chem. Eng. J. 171 (2), 711–716.